

## Spatiotemporal GLP-1 and GIP receptor signaling and trafficking/recycling dynamics induced by selected receptor mono- and dual-agonists

Aaron Novikoff, Shannon L. O'Brien, Miriam Bernecker, Gerald Grandl, Maximilian Kleinert, Patrick J. Knerr, Kerstin Stemmer, Martin Klingenspor, Anja Zeigerer, Richard DiMarchi, Matthias H. Tschöp, Brian Finan, Davide Calebiro, Timo D. Müller

### Angaben zur Veröffentlichung / Publication details:

Novikoff, Aaron, Shannon L. O'Brien, Miriam Bernecker, Gerald Grandl, Maximilian Kleinert, Patrick J. Knerr, Kerstin Stemmer, et al. 2021. "Spatiotemporal GLP-1 and GIP receptor signaling and trafficking/recycling dynamics induced by selected receptor mono- and dual-agonists." *Molecular Metabolism* 49.  
<https://doi.org/10.1016/j.molmet.2021.101181>.

# Spatiotemporal GLP-1 and GIP receptor signaling and trafficking/recycling dynamics induced by selected receptor mono- and dual-agonists



Aaron Novikoff<sup>1,2,3,14</sup>, Shannon L. O'Brien<sup>4,5,14</sup>, Miriam Bernecker<sup>1,2</sup>, Gerald Grandl<sup>1,2</sup>, Maximilian Kleinert<sup>1,2</sup>, Patrick J. Knerr<sup>6</sup>, Kerstin Stemmer<sup>1,2</sup>, Martin Klingenspor<sup>7</sup>, Anja Zeigerer<sup>2,8,9</sup>, Richard DiMarchi<sup>10</sup>, Matthias H. Tschöp<sup>2,3,11,12</sup>, Brian Finan<sup>6</sup>, Davide Calebiro<sup>4,5,\*,14</sup>, Timo D. Müller<sup>1,2,13,\*,14</sup>

## ABSTRACT

**Objective:** We assessed the spatiotemporal GLP-1 and GIP receptor signaling, trafficking, and recycling dynamics of GIPR mono-agonists, GLP-1R mono-agonists including semaglutide, and GLP-1/GIP dual-agonists MAR709 and tirzepatide.

**Methods:** Receptor G protein recruitment and internalization/trafficking dynamics were assessed using bioluminescence resonance energy transfer (BRET)-based technology and live-cell HILO microscopy.

**Results:** Relative to native and acylated GLP-1 agonists, MAR709 and tirzepatide showed preserved maximal cAMP production despite partial  $G\alpha_s$  recruitment paralleled by diminished ligand-induced receptor internalization at both target receptors. Despite MAR709's lower internalization rate, GLP-1R co-localization with Rab11-associated recycling endosomes was not different between MAR709 and GLP-1R specific mono-agonists.

**Conclusions:** Our data indicated that MAR709 and tirzepatide induce unique spatiotemporal GLP-1 and GIP receptor signaling, trafficking, and recycling dynamics relative to native peptides, semaglutide, and matched mono-agonist controls. These findings support the hypothesis that the structure of GLP-1/GIP dual-agonists confer a biased agonism that, in addition to its influence on intracellular signaling, uniquely modulates receptor trafficking.

© 2021 The Authors. Published by Elsevier GmbH. This is an open access article under the CC BY license (<http://creativecommons.org/licenses/by/4.0/>).

**Keywords** GLP-1R; GIPR; Biased agonism; Receptor Internalization; Receptor Trafficking; Dual-agonists

## 1. INTRODUCTION

Glucagon-like peptide-1 (GLP-1) is a pleiotropic hormone with broad pharmacological potential due to its ability to improve body weight, food intake, and glucose metabolism [1]. However, active GLP-1, which is primarily GLP-1 (7–36 amide) and to a lower extent GLP-1 (7–37), is subject to rapid proteolytic degradation and fast renal elimination [2–5]. Long-acting analogs with biochemical modifications in the GLP-1 sequence have been designed to overcome these

limitations and are in clinical use for treating type 2 diabetes [6,7]. Despite molecular enhancements in time action, dose-dependent adverse effects limit the maximal efficacy and overall therapeutic potential of GLP-1R mono-agonists [8]. Single chimeric molecules with dual agonism at the receptors for GLP-1 and glucose-dependent insulinotropic polypeptide (GIP) improve body weight and glucose handling with superior potency to GLP-1R mono-agonists in preclinical [9,10] and clinical studies [11]. While GLP-1/GIP dual-agonists have advanced to phase 3 clinical trials for treating obesity and diabetes, the

<sup>1</sup>Institute for Diabetes and Obesity, Helmholtz Diabetes Center, Helmholtz Zentrum München, Neuherberg, Germany <sup>2</sup>German Center for Diabetes Research (DZD), Neuherberg, Germany <sup>3</sup>Division of Metabolic Diseases, Department of Medicine, Technische Universität München, D-80333 Munich, Germany <sup>4</sup>Institute of Metabolism and Systems Research, University of Birmingham, Birmingham, B15 2TT, UK <sup>5</sup>Center of Membrane Proteins and Receptors (COMPARE), Universities of Nottingham and Birmingham, Birmingham, B15 2TT, UK <sup>6</sup>Novo Nordisk Research Center Indianapolis, Indianapolis, IN 46241, USA <sup>7</sup>Chair for Molecular Nutritional Medicine, School of Life Sciences, Technical University of Munich, 85354 Freising, Germany <sup>8</sup>Institute for Diabetes and Cancer, Helmholtz Center Munich, 85764 Neuherberg, Germany <sup>9</sup>Joint Heidelberg-IDC Translational Diabetes Program, Inner Medicine 1, Heidelberg University Hospital, Heidelberg, Germany <sup>10</sup>Department of Chemistry, Indiana University, Bloomington, IN 47405, USA <sup>11</sup>Helmholtz Zentrum München, Neuherberg, Germany <sup>12</sup>Technische Universität München, München, Germany <sup>13</sup>Department of Pharmacology and Experimental Therapy, Institute of Experimental and Clinical Pharmacology and Toxicology, Eberhard Karls University Hospitals and Clinics, 72076 Tübingen, Germany

<sup>14</sup> These authors contributed equally to this work.

\*Corresponding author. Institute for Diabetes and Obesity, Helmholtz Diabetes Center, Helmholtz Zentrum München, Neuherberg, Germany. E-mail: [timo.mueller@helmholtz-muenchen.de](mailto:timo.mueller@helmholtz-muenchen.de) (T.D. Müller).

\*\*Corresponding author. Institute of Metabolism and Systems Research, University of Birmingham, Birmingham, B15 2TT, UK. E-mail: [D.Calebiro@bham.ac.uk](mailto:D.Calebiro@bham.ac.uk) (D. Calebiro).

Received August 8, 2020 • Revision received January 29, 2021 • Accepted January 30, 2021 • Available online 6 February 2021

<https://doi.org/10.1016/j.molmet.2021.101181>

contribution of GIPR agonism to these applications is questionable. Mice with GIP receptor (GIPR) depletion are protected from diet-induced obesity [12], and patients with type 2 diabetes show an impaired insulinotropic response to GIP infusion [13]. Antibodies antagonizing GIPR improve body weight and glucose metabolism in obese rodents and non-human primates [14]. Recent hypotheses to reconcile these discrepancies include GIPR agonists acting as functional GIPR antagonists, or alternatively that specific ligands engage unique receptor signaling, trafficking, and/or recycling dynamics, commonly referred to as biased-agonism [15]. Biased agonism at the GLP-1R has been linked to differential cellular desensitization capacities via differences in receptor internalization and/or  $\beta$ -arrestin recruitment, as has been shown for Phe1-substituted exendin-4 [16]. In addition to the GLP-1R agonists exendin-4 and oxyntomodulin, both of which demonstrate bias toward  $\beta$ -arrestin recruitment [17],  $\alpha$ / $\beta$  amino acid modifications to the GLP-1 backbone sequence can also result in differential GLP-1R signaling [18]. Likewise, the GLP-1/GIP dual-agonist tirzepatide (LY3298176; Eli Lilly, Indianapolis, IN, USA) was recently reported to favor phosphorylation of ERK1/2 relative to  $\beta$ -arrestin and  $G\alpha_s$  protein at both target receptors [19]. The aim of this study was to assess the spatiotemporal GLP-1 and GIP receptor signaling, trafficking, and recycling dynamics mediated by select GLP-1R and GIPR mono- and dual-agonists. MAR709 is characterized as a balanced GLP-1/GIP co-agonist and is acylated with a C16 fatty mono-acid, which allows for once-daily time action in humans [20,21]. Tirzepatide is characterized as an imbalanced GLP-1/GIP co-agonist that favors GIPR potency and is acylated with a C20 fatty di-acid at position 20, which allows for once-weekly time action in humans [22]. Our results show that both dual-agonists, MAR709 and tirzepatide, act as partial effectors at GLP-1R for G protein recruitment, receptor internalization,  $\beta$ -arrestin recruitment, Rab5<sup>+</sup>/Rab7<sup>+</sup> receptor trafficking, and endosomal G-protein recruitment, while retaining full-agonist capacity for cAMP production. Interestingly, despite showing a reduced receptor internalization rate, MAR709 acts as a full effector for stimulating GLP-1R incorporation into Rab11<sup>+</sup> recycling endosomes. At the GIP receptor, dual-agonists similarly act as full agonists for cAMP, but lack the G protein recruitment partial agonism profile and display limited receptor internalization and trafficking properties. Our data support the hypothesis that biased agonism with unique receptor signaling and trafficking properties might be a potential basis for enhanced metabolic benefits of these GLP-1/GIP dual-agonists.

## 2. METHODS

### 2.1. Plasmids

Untagged human GLP-1R was purchased from Sino Biological Inc. (Cat #: HG13944-UT, Beijing, China) and untagged human GIPR and human GIPR-turbo GFP were purchased from OriGene Technologies Inc. (Cat #: SC110906 and RG210811, Rockville, MD, USA). Human GLP-1R-GFP was a gift from Professor David Hodson (University of Birmingham, Birmingham, UK). Human GLP-1R-Rluc8 (hGLP-1R-Rluc8) was a gift from Professor Patrick Sexton (Monash University, Melbourne, Australia). Human CMV-GIPR-Rluc8 (hGIPR-Rluc8) with VSLGSSG residues was constructed and purchased from VectorBuilders Inc. (Neu-Isenburg, Germany). cAMP sensor pcDNA3L-His-CAMYEL (ATCC MBA-277TM) was purchased from ATCC (Manassas, VA, USA) [23]. NES-Nluc-mini-G plasmids ( $G\alpha_s$ ,  $G\alpha_q$ ,  $G\alpha_i$ , and  $G\alpha_{12/13}$ ) and subcellular/endosomal markers Rab GTPases (Rabs) Venus-Rab5a (early endosomes), Venus-Rab7a (late endosomes/lysosomes), Venus-Rab11a (recycling endosomes), and Venus-KRAS (plasma membrane) were gifts from Kevin

Pfleger (Harry Perkins Institute of Medical Research, Nedlands, WA, Australia) as originally published by Professor Nevin Lambert (Augusta University, Augusta, GA, USA) [24].  $\beta$ -arrestin 1/2-Rluc8 plasmids were a gift from Professor Terry Hébert (McGill University, Montreal, Canada).

### 2.2. Peptide synthesis

Semaglutide was provided by Novo Nordisk (Bagsværd, Denmark). All of the other peptides were prepared via standard automated Fmoc/tBu solid-phase peptide synthesis on Rink Amide ChemMatrix resin. An orthogonal protecting group strategy was used to incorporate the protraction moiety onto the appropriate lysine side chain. Following synthesis, crude compounds were cleaved from the resin with 95:2.5:2.5 trifluoroacetic acid/water/triisopropylsilane. The crude compounds were purified by reversed-phase high-performance liquid chromatography (RP-HPLC) on a Luna C8 (2) preparative column with a gradient of water/acetonitrile containing 0.1% trifluoroacetic acid, then lyophilized to produce the desired compounds as white powders. Compound identity was confirmed via RP-HPLC-mass spectrometry. hGLP-1 (7–36 amide) was purchased from Anaspec (Cat #: AS-22463, Fremont, CA, USA). hGIP (1–42) was purchased from Anaspec (Cat #: AS-61226-1, Fremont, CA, USA).

### 2.3. Cell culture

HEK293T cells lacking endogenous GLP-1R and GIPR were cultured in Dulbecco's Modified Eagle Medium (DMEM, Cat #: 11995073, Life Technologies, Carlsbad, CA, USA) with 10% heat-inactivated fetal bovine serum (FBS, Cat #: 10500064, Life Technologies, Carlsbad, CA, USA), 100 IU/mL of penicillin, and 100  $\mu$ g/mL of streptomycin solution (Pen-Strep, Cat #: P4333, Sigma–Aldrich, St. Louis, MO, USA). Min6 cells were cultured in Dulbecco's Modified Eagle Medium with 15% heat-inactivated fetal bovine serum, 100 IU/mL of penicillin, 100  $\mu$ g/mL of streptomycin solution, 20 mM of HEPES, and 50  $\mu$ M of  $\beta$ -mercaptoethanol. All of the cells were maintained at 37 °C in 5% CO<sub>2</sub>.

### 2.4. Ligand-induced BRET assay

The cells were seeded (700,000 cells/well) in 6-well plates and incubated to ~70% confluency in complete media supplemented with 10% FBS and 1% Pen-Strep. Twenty-four hours after seeding, over-expression of target proteins was performed under transient transfection conditions using Lipofectamine 2000 (Cat #: 11668019, Invitrogen, Carlsbad, CA, USA) according to the manufacturer's protocol without including additional carrier DNA. Twenty-four hours after transfection, the cells were washed with PBS, then detached and resuspended in FluoroBrite phenol red-free complete media (Cat #: A1896701, Life Technologies, Carlsbad, CA, USA) containing 5% FBS and 2 mM of L-glutamine (Cat #: 25030081, Life Technologies, Carlsbad, CA, USA). Then 100,000 cells/well were plated into poly-D-lysine-coated (Cat #: P6403, Sigma–Aldrich, St. Louis, MO, USA) 96-well white polystyrene LumiNunc microplates (Cat #: 10072151, Thermo Fisher Scientific, Waltham, MA, USA). After 24 h, the media was replaced with PBS (Cat #: 10010056, Gibco, Carlsbad, CA, USA) containing 10  $\mu$ M of coelenterazine-h (Cat #: S2011, Promega, Madison, WI, USA) or 1:500 NanoGlo (Cat #: N1110, Promega, Madison, WI, USA). BRET<sup>1</sup> measurements were taken every 30 s for 2 min at 37 °C using a PHERAstar FS multi-mode microplate reader with 430–485 nm and 505–590 nm dual filters. Baseline measurements were taken after 5 min of incubation with coelenterazine-h or NanoGlo. The cells were then treated with a vehicle or the respective agonists. The resulting ratiometric BRET signal between the interacting fluorophore and lumiphore was normalized by subtracting the background ratio (505–590 nm emission over 430–485 nm) of the

vehicle-treated wells with the matched agonist-treated wells producing a signal defined as the “ligand-induced BRET ratio” [25]. The temporal data of the vehicle-corrected agonist measurement was then normalized to the baseline reading of the same well. The first BRET reading following treatment with agonist/vehicle was the subsequent measurement after the zero time point. Positive or negative incremental areas under the curves (+iAUC/-iAUC) were calculated where noted. Each experiment was independently performed at least three times, with at least two technical replicates for each group.

### 2.5. G-protein recruitment assay

Mini-G protein probes translocate to ligand-bound active receptors retaining their specificity (Wan et al., 2018). To measure the ligand-induced recruitment of the  $G\alpha_s$ ,  $G\alpha_q$ ,  $G\alpha_i$ , and  $G\alpha_{12/13}$ , 50 ng DNA of the respective NLuc-tagged mini-G plasmid was co-transfected with 500 ng DNA of GLP-1R GFP or GIPR-GFP per well of a 6-well plate.

### 2.6. cAMP assay

CAMYEL, a cAMP sensor using YFP-Epac-RLuc [23] was utilized to quantify cAMP accumulation with the temporal resolution. Then, 500 ng of CAMYEL DNA was co-transfected with 500 ng of DNA of untagged GLP-1R or GIPR per well in a 6-well plate. The experiments were performed in the absence of 3-isobutyl-1-methylxanthine (IBMX).

### 2.7. GPCR internalization assay

A GPCR internalization assay was established by measuring the loss of baseline resonance energy transfer between an intracellular plasma membrane marker Venus-KRAS and hGLP-1R-RLUC8 or hGIPR-RLUC8 [26]. Then, 500 ng of Venus-KRAS DNA and 300 ng of the respective RLUC8-tagged GPCR DNA were used per well in a 6-well plate.

### 2.8. $\beta$ -arrestin recruitment assay

Co-localization of  $\beta$ -arrestin1/2-RLUC8 with GLP-1R-GFP or GIPR-GFP was assessed [27]. Fifty ng of  $\beta$ -arrestin1-RLUC8 or  $\beta$ -arrestin2-RLUC8 DNA and 300 ng of GLP-1R-GFP or GIPR-GFP DNA were co-transfected into each well in a 6-well plate.

### 2.9. Endosomal trafficking assay

GPCR endosomal trafficking [28] was assessed by measuring the ligand-stimulated gain in resonance energy transfer between Venus-Rab5/7/11 and hGLP-1R-RLUC8 or hGIPR-RLUC8. Then, 100 ng of the respective Venus-Rab subtype DNA and 100 ng of hGLP-1R-RLUC8 or hGIPR-RLUC8 DNA were co-transfected into each well in a 6-well plate.

### 2.10. Endosomal G-protein recruitment assay

Endosomal G-protein recruitment was assessed by bystander BRET via GPCR-induced co-localization of  $G\alpha_s$ -NLuc with Venus-Rab5/7/11. Then, 300 ng of GLP-1R-untagged or GIPR-untagged DNA, 500 ng of Venus-Rab5/7/11 DNA, and 50 ng of  $G\alpha_s$ -NLuc DNA were co-transfected per well in a 6-well plate.

### 2.11. HILO microscopy

HEK293T cells were seeded onto 24 mm coverslips (Cat #: 631–1584, VWR, Radnor, PA, USA) and transfected with 500 ng of GLP-1R-GFP or GIPR-GFP over 24 h. HILO image sequences were acquired with a custom-built TIRF microscope (Cairn Research) based on an Eclipse Ti2 (Nikon, Tokyo, Japan) equipped with an EMCCD camera (iXon Ultra, Andor), a 488 nm diode laser, a hardware Perfect Focus System, a

TIRF iLas2 module, and a 100 $\times$  oil-immersion objective (NA 1.49, Nikon). Coverslips were mounted onto metal imaging chambers with a plastic seal and filled with imaging medium (HBSS supplemented with 10 mM of HEPES). The objective and samples were maintained at 37 °C in a heated enclosure. Images were acquired on MetaMorph software (Molecular Devices) using a frame exposure of 50–200 ms with an image acquired before ligand stimulation and a subsequent image taken every 30 s thereafter, up to 20 min. All of the images were analyzed using ImageJ.

### 2.12. Data analysis

Data are represented as means  $\pm$  S.E.M. Each experiment was independently conducted at least three times, each with at least two technical replicates.  $E_{\max}$  values were normalized to GLP-1 (7–36 amide) or GIP (1–42). Dose responses were fitted using non-linear regression. pEC50 and EC50 values were calculated using GraphPad Prism 8.0 (GraphPad, San Diego, CA, USA). Statistical analyses were calculated in GraphPad 8.0 using one-way analysis of variance (ANOVA) and corrected with Tukey's or Bonferroni's multiple comparison test. Differences are considered significant with an adjusted p value < 0.05.

## 3. RESULTS

### 3.1. MAR709 and tirzepatide differed from GLP-1R and GIPR mono-agonists in G protein recruitment

Ligand-induced (1  $\mu$ M) capacity for receptor G protein recruitment was assessed using bioluminescence resonance energy transfer (BRET)-based technology in HEK293T cells transiently transfected with the respective GFP-tagged receptors and mini-G constructs. The molecules evaluated included the native ligands GLP-1 (7–36 amide) and GIP (1–42), semaglutide (Novo Nordisk, Copenhagen, Denmark), the GLP-1/GIP dual-agonists tirzepatide (Eli Lilly, Indianapolis, IN, USA) and MAR709 (Novo Nordisk, Copenhagen, Denmark), and two molecules (fatty acyl-GLP-1 and fatty acyl-GIP) that are derived from the MAR709 sequence but had been structurally modified via single- or double-point mutations to only activate either GLP-1R or GIPR (Figure 1). A table including the external company identifiers, in-text abbreviations, and amino acid sequence structures of the agonists is available (Supplementary Table 1).

In GLP-1R<sup>+</sup> HEK293T cells, GLP-1 (7–36 amide) strongly recruited  $G\alpha_s$  and to a lesser extent  $G\alpha_q$ , with no meaningful recruitment of  $G\alpha_i$  and  $G\alpha_{12/13}$  (Figure 2A–D). GIP (1–42) and fatty acyl-GIP did not stimulate G protein recruitment in GLP-1R<sup>+</sup> HEK293T cells, while semaglutide and fatty acyl-GLP-1 elicited comparable responses relative to GLP-1 (7–36 amide) (Figure 2A–D). Relative to the GLP-1 mono-agonists, both GLP-1/GIP dual-agonists showed a decreased ability to recruit  $G\alpha_s$  and  $G\alpha_q$ , however, MAR709 demonstrated a higher capacity to recruit  $G\alpha_s$  and  $G\alpha_q$  compared to tirzepatide (Figure 2A,B). The chimeric structures of MAR709 and tirzepatide did not additionally diversify the G-protein families recruited to the receptor as evidenced by a lack of  $G\alpha_i$  and  $G\alpha_{12/13}$  recruitment (Figure 2A–D). In GIPR<sup>+</sup> HEK293T cells, native GIP (1–42) predominantly recruited  $G\alpha_s$  without meaningful recruitment of  $G\alpha_q$ ,  $G\alpha_i$ , and  $G\alpha_{12/13}$  (Figure 2E–H). As expected, GLP-1 (7–36 amide), fatty acyl-GLP-1 and semaglutide all showed negligible effects on G protein recruitment in the absence of GLP-1R (Figure 2E–H). Relative to native GIP (1–42),  $G\alpha_s$  recruitment following treatment with fatty acyl-GIP and tirzepatide was comparable, but with MAR709 it slightly decreased (Figure 2E).

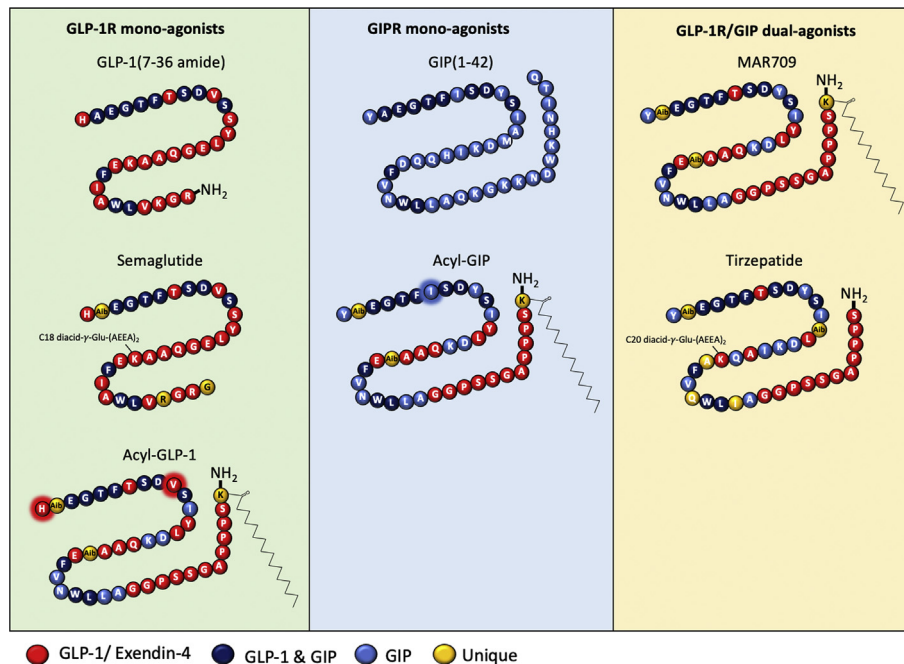


**Figure 1: Schematic and structure of the tested GLP-1R and GIPR ligands.** GLP-1R mono-agonists comprised of human GLP-1 (7–36 amide), semaglutide, and fatty acyl-GLP-1 (a pharmacokinetically-matched His1 and Val10 mutant of MAR709) (left panel). GIPR mono-agonists include human GIP (1–42) and fatty acyl-GIP (a pharmacokinetically matched Ile7 mutant of MAR709) (middle panel). GLP-1/GIP dual-agonist MAR709 and tirzepatide (right panel).

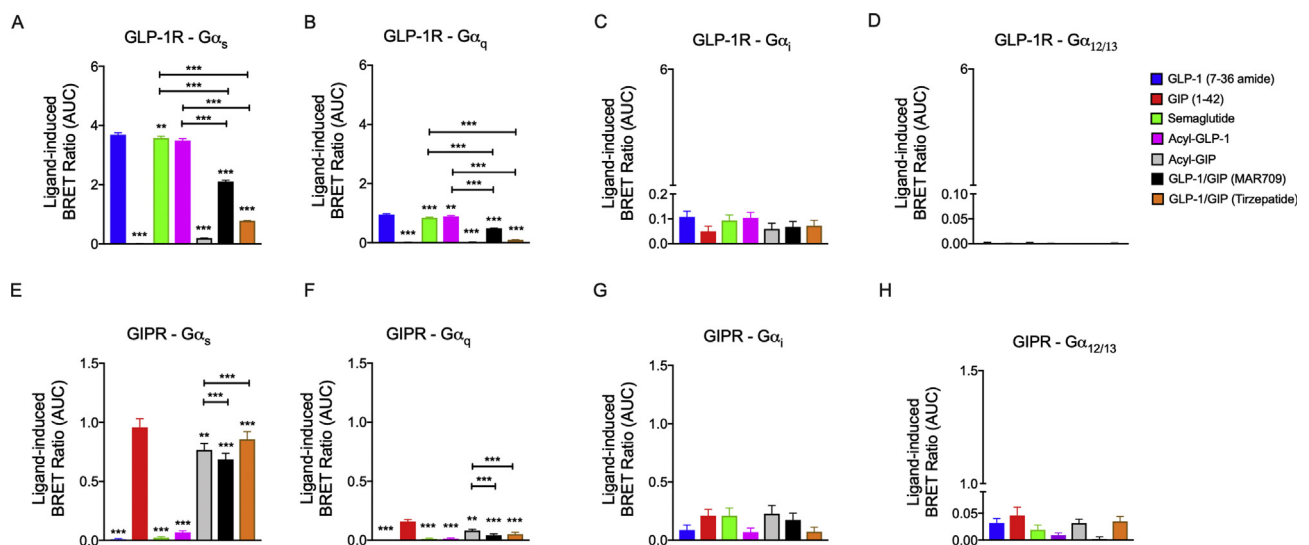


**Figure 2: Ligand-induced G protein recruitment at GLP-1R and GIPR.** Ligand-induced (1  $\mu$ M) recruitment of Nluc-tagged  $G\alpha_s$  (A),  $G\alpha_q$  (B),  $G\alpha_i$  (C), and  $G\alpha_{12/13}$  (D) to GFP-tagged GLP-1R in HEK293T cells. Ligand-induced (1  $\mu$ M) recruitment of Nluc-tagged  $G\alpha_s$  (E),  $G\alpha_q$  (F),  $G\alpha_i$  (G), and  $G\alpha_{12/13}$  (H) with GFP-tagged GIPR<sup>+</sup> HEK293T cells. The positive iAUC (+iAUC) representation of vehicle and baseline-corrected 30 min response to each agonist is expressed as mean  $\pm$  SEM. Bonferroni's test, \* $p$  < 0.05, \*\* $p$  < 0.005, and \*\*\* $p$  < 0.0005 using one-way ANOVA vs GLP-1 (7–36 amide) or GIP (1–42). Three independent experiments were performed with at least two technical replicates per group.

In summary, the GLP-1 mono-agonists and GLP-1/GIP dual-agonists primarily initiated  $G\alpha_s$  recruitment, and to a lesser extent  $G\alpha_q$ , at the GLP-1R and GIPR. In relation to the GLP-1 mono-agonists, both GLP-1/GIP dual-agonists showed decreased  $G\alpha_s$  and  $G\alpha_q$  recruitment in GLP-1R<sup>+</sup> HEK293T cells. In GIPR<sup>+</sup> cells, tirzepatide led to comparable recruitment of  $G\alpha_s$  relative to native GIP while MAR709 showed a slight decrease in  $G\alpha_s$  recruitment.

### 3.2. MAR709 and tirzepatide were partial agonists for $G\alpha_s$ recruitment at GLP-1R but full agonists for cAMP production

We next assessed concentration-response dependence in ligand-induced  $G\alpha_s$  recruitment and evaluated how this capacity translated to cAMP production. At all of the tested concentrations, semaglutide and fatty acyl-GLP-1 showed comparable  $G\alpha_s$  recruitment relative to native GLP-1 (7–36 amide) in GLP-1R<sup>+</sup> cells (Figure 3A). In line with



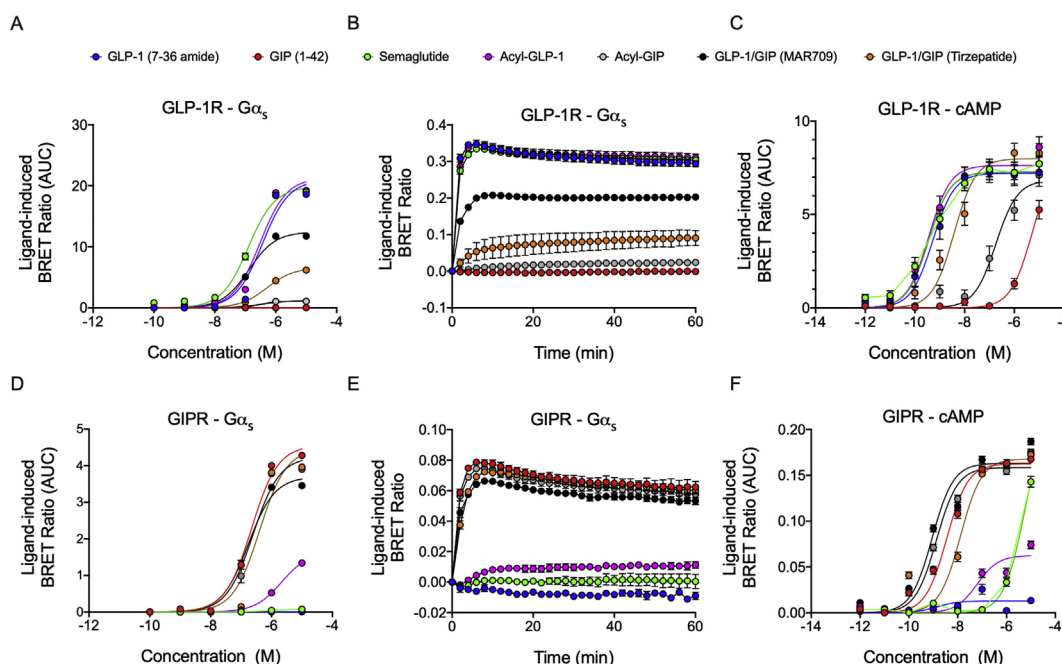


**Figure 3:** Dose-dependent effects of ligands on  $G\alpha_s$  recruitment and cAMP production. Dose–response curves (A) and temporal resolution (1  $\mu$ M stimulation) (B) of ligand-induced BRET changes between Nluc-tagged  $G\alpha_s$  recruitment to GFP-tagged GLP-1R. Dose–response curves of ligand-induced cAMP production GLP-1R<sup>+</sup> HEK293T cells (C). Dose–response curves (D) and temporal resolution (1  $\mu$ M stimulation) (E) of ligand-induced  $G\alpha_s$  recruitment to the GIPR. Dose–response curves of ligand-induced cAMP production GIPR<sup>+</sup> HEK293T cells (F). +iAUC representation of vehicle and baseline-corrected 60 min ( $G\alpha_s$  recruitment) or 25 min (cAMP generation) temporal responses to each agonist is expressed as mean  $\pm$  SEM. Three independent experiments were performed with at least two technical replicates per group.

our previous data (Figure 2A), MAR709 and tirzepatide both acted as partial agonists at the GLP-1R, stimulating a respective 59% and 31% maximal  $G\alpha_s$  recruitment ( $E_{max}$ ) relative to GLP-1 (7–36 amide) (Figure 3A and Table 1). This partial agonism was independent of the measurement time after drug exposure (Figure 3B). Interestingly, despite a reduced  $G\alpha_s$  recruitment  $E_{max}$ , the dual-agonists did not differ in cAMP  $E_{max}$  compared to the GLP-1 mono-agonists (Figure 3C and Table 1). This was further validated with a CAMYEL sensor saturation assay (Supplementary Figure 4A–C), with ligand responses falling below the saturation limit of the sensor. Hence, despite partial agonism at the level of G protein recruitment to GLP-1R, the dual-agonists remained full agonists when considering cAMP generation. In terms of potency, all of the agonists displayed similar cAMP pEC50 values except for tirzepatide, which was significantly decreased relative to GLP-1 (7–36 amide) (Figure 3C and Table 1).

In GIPR<sup>+</sup> HEK293T cells, we observed a comparable potency and efficacy for  $G\alpha_s$  recruitment upon treatment with fatty acyl-GIP and both dual-agonists relative to native GIP (1–42) (Figure 3D and Table 1), which was independent of the measurement time after drug exposure (Figure 3E). MAR709 exhibited a slightly reduced efficacy at the GIPR, stimulating 81% of the  $G\alpha_s$  recruitment  $E_{max}$  elicited by native GIP (1–42) (Figure 3D and Table 1). For cAMP production, both fatty acyl-GIP and MAR709 displayed a significantly superior pEC50 than that of GIP (1–42), while tirzepatide exhibited a significant 3-fold reduction in potency (Figure 3F and Table 1). Collectively, MAR709 and tirzepatide displayed unique agonism properties at their target receptors, retaining full cAMP efficacy at both the GLP-1R and GIPR despite relatively lower GLP-1R-specific  $G\alpha_s$  recruitment efficacy and a slightly reduced relative potency of tirzepatide for cAMP production at the GIP receptor.

### 3.3. MAR709 and tirzepatide showed decreased receptor internalization relative to GLP-1R and GIPR mono-agonists

We next assessed ligand-induced receptor internalization and the recruitment of  $\beta$ -arrestin and  $G\alpha_q$ . In hGLP-1R-Rluc8<sup>+</sup> HEK293T cells, semaglutide and fatty acyl-GLP-1 showed similar receptor internalization dynamics relative to GLP-1 (7–36 amide) (Figure 4A,B). However, both MAR709 and tirzepatide showed strikingly decreased receptor internalization compared to the tested GLP-1R mono-agonists (Figure 4A,B). Relative to GLP-1 (7–36 amide), the maximal ligand-induced GLP-1R internalization ( $E_{max}$ ) of MAR709 and tirzepatide was 51% and 13%, respectively (Figure 4A,B and Table 1). Likewise, decreased internalization of GLP-1R was also observed upon treatment of hGLP-1R-Rluc8<sup>+</sup> Min6 cells with MAR709 and tirzepatide relative to GLP-1 (7–36 amide) and GLP-1 mono-agonists (Supplementary Figure 5A–C). No significant differences were observed in the pEC50 values of the tested ligands in HEK293T cells. Decreased receptor internalization mediated by MAR709 and tirzepatide was also confirmed using live cell HILO microscopy in HEK293T cells expressing GLP-1R-GFP (Figure 4C). While treatment with GLP-1 (7–36 amide) and semaglutide initiated rapid internalization of GLP-1R-GFP, MAR709 and tirzepatide showed the persistent presence of the ligand–receptor complex at the plasma membrane with strikingly less trafficking into the cytosol (Figure 4C). These data collectively demonstrated that MAR709 and tirzepatide differed from the GLP-1R mono-agonists in that they showed prolonged receptor presence at the cell surface and reduced receptor internalization.

GLP-1R recruitment of  $\beta$ -arrestin 1/2 ( $\beta$ -arr1/2) has been shown to influence receptor trafficking and enhance extracellular signal-regulated kinase 1/2 (ERK1/2) signaling [29]. In GLP-1R<sup>+</sup> HEK293T cells, semaglutide stimulated 67% and 78% of the  $\beta$ -arr1 and  $\beta$ -arr2

**Table 1 — Maximal ( $E_{\max}$ ) drug effects and affinities at the GLP-1R or GIPR target receptors.** Data were generated in HEK293T cells transiently transfected to express GLP-1R or GIPR.  $E_{\max}$ , pEC50, and EC50 values were generated from dose–response values fitted to sigmoidal curves using a three-parameter non-linear logistic regression. The  $E_{\max}$  is the maximal response elicited by an agonist and is expressed as % of the maximum response of GLP-1 (7–36 amide) or GIP (1–42). The EC50 is the molar concentration in which an agonist produced half of the maximal response. The pEC50 is the negative logarithm of the EC50. Values are given for  $G\alpha_s$  recruitment, cAMP accumulation, receptor internalization,  $\beta$ -arrestin  $1/2$ , and  $G\alpha_q$  recruitment at the GLP-1R and the GIPR. All of the values were derived from the iAUC of a temporal response for each concentration/agonist and are expressed as mean  $\pm$  SEM from at least 3 independent experiments with at least two technical replicates per group. Statistical significance was determined using one-way ANOVA and corrected with Bonferroni's multiple comparisons test.  $^{*}/\dagger p < 0.05$ .  $^{*}$  vs GLP-1 (7–36 amide) or GIP (1–42).  $^{\#}$  vs semaglutide.  $^{\dagger}$  vs fatty acyl-GLP-1 or fatty acyl-GIP. NA = no agonism significantly different than zero observed at 1  $\mu$ M stimulation. Bold red = with significant non-zero agonism at 1  $\mu$ M stimulation but incomplete curve fit, last value at 10  $\mu$ M used.

	cAMP			$G\alpha_s$ Recruitment			Receptor Internalization			$\beta$ -arr1 Recruitment			$\beta$ -arr2 Recruitment			$G\alpha_q$ Recruitment		
	$E_{\max}$ (% GLP-1)	pEC50	EC50 (nM)	$E_{\max}$ (% GLP-1)	pEC50	EC50 (nM)	$E_{\max}$ (% GLP-1)	pEC50	EC50 (nM)	$E_{\max}$ (% GLP-1)	pEC50	EC50 (nM)	$E_{\max}$ (% GLP-1)	pEC50	EC50 (nM)	$E_{\max}$ (% GLP-1)	pEC50	EC50 (nM)
<b>GLP-1R</b>																		
Native GLP-1 (7–36 amide)	100 $\pm$ 3	9.28 $\pm$ 0.11	5229	100 $\pm$ 6	6.44 $\pm$ 0.12	361.8	100 $\pm$ 7	6.37 $\pm$ 0.15	422.5	100 $\pm$ 6	6.37 $\pm$ 0.12	427.4	100 $\pm$ 3	6.64 $\pm$ 0.06	231.6	100 $\pm$ 6	6.38 $\pm$ 0.39	420.9
GIP (1–42)	NA	NA	NA	NA	NA	NA	NA	NA	NA	NA	NA	NA	NA	NA	NA	NA	NA	NA
Semaglutide	101 $\pm$ 3 [†]	9.44 $\pm$ 0.12	3613	95 $\pm$ 2 [5]	6.90 $\pm$ 0.05	130.3	107 $\pm$ 5 [7]	6.27 $\pm$ 0.09	528.1	67 $\pm$ 4 [33]	6.58 $\pm$ 0.13	264.5	78 $\pm$ 3 [22]	6.78 $\pm$ 0.09	164.4	98 $\pm$ 5 [2]	6.41 $\pm$ 0.33	389.5
Acyl GLP-1	106 $\pm$ 3 [†]	9.44 $\pm$ 0.11	3602	101 $\pm$ 5 [1]	6.52 $\pm$ 0.10	304.5	108 $\pm$ 4 [8]	6.41 $\pm$ 0.08	391.6	95 $\pm$ 6 [5]	6.42 $\pm$ 0.13	383.6	86 $\pm$ 3 [14]	6.72 $\pm$ 0.07	187.7	98 $\pm$ 7 [2]	6.37 $\pm$ 0.43	423.8
Acyl GIP	NA	6.74 $\pm$ 0.14	181.2	NA	NA	NA	NA	NA	NA	NA	NA	NA	NA	NA	NA	NA	NA	NA
Dual Agonist (Mar709)	100 $\pm$ 3 [†]	9.44 $\pm$ 0.10	3613	59 $\pm$ 1 [41]	6.88 $\pm$ 0.04	131.2	51 $\pm$ 2 [49]	6.14 $\pm$ 0.06	728.8	35 $\pm$ 1 [65]	6.52 $\pm$ 0.08	301.7	24 $\pm$ 1 [78]	6.92 $\pm$ 0.12	119.2	48 $\pm$ 3 [52]	6.36 $\pm$ 0.21	432.2
Dual Agonist (Tirzepatide)	110 $\pm$ 4 [†]	8.42 $\pm$ 0.11	3.766	31 $\pm$ 1 [69]	6.29 $\pm$ 0.05	514.5	13 $\pm$ 1 [87]	6.21 $\pm$ 0.13	623.7	NA	NA	NA	NA	NA	NA	17 $\pm$ 1 [53]	6.23 $\pm$ 0.06	587.5
<b>GIPR</b>																		
Native GLP-1 (7–36 amide)	NA	NA	NA	NA	NA	NA	NA	NA	NA	NA	NA	NA	NA	NA	NA	NA	NA	NA
GIP (1–42)	100 $\pm$ 2	8.45 $\pm$ 0.07	3.573	100 $\pm$ 2	6.65 $\pm$ 0.10	219.2	100 $\pm$ 3	7.43 $\pm$ 0.07	37.23	NA	NA	NA	<b>100 <math>\pm</math> 18 (10 <math>\mu</math>M)</b>	<b>6.77 <math>\pm</math> 0.39</b>	NA	100 $\pm$ 5	6.55 $\pm$ 0.04	283.3
Semaglutide	NA	NA	NA	NA	NA	NA	NA	NA	NA	NA	NA	NA	NA	NA	NA	NA	NA	NA
Acyl GLP-1	NA	NA	NA	NA	NA	NA	NA	NA	NA	NA	NA	NA	NA	NA	NA	NA	NA	NA
Acyl GIP	97 $\pm$ 3 [3]	8.87 $\pm$ 0.07	1.342	93 $\pm$ 3 [7]	6.61 $\pm$ 0.15	247.2	11 $\pm$ 2 [89]	8.54 $\pm$ 0.04	2.854	NA	NA	NA	NA	NA	NA	90 $\pm$ 3 [10]	6.99 $\pm$ 0.03	101.4
Dual Agonist (Mar709)	100 $\pm$ 3 [†]	9.05 $\pm$ 0.10	899.1	81 $\pm$ 2 [19]	6.77 $\pm$ 0.09	171.3	4 $\pm$ 2 [96]	9.99 $\pm$ 0.03	0.103	NA	NA	NA	<b>36 <math>\pm</math> 25 [64]</b>	<b>7.41 <math>\pm</math> 0.23</b>	NA	68 $\pm$ 3 [32]	6.82 $\pm$ 0.03	152.7
Dual Agonist (Tirzepatide)	103 $\pm$ 5 [†]	7.88 $\pm$ 0.13	13.07	97 $\pm$ 6 [3]	6.39 $\pm$ 0.28	405	18 $\pm$ 1 [82]	8.33 $\pm$ 0.03	4.665	NA	NA	NA	<b>35 <math>\pm</math> 14 [65]</b>	<b>7.49 <math>\pm</math> 0.40</b>	NA	85 $\pm$ 3 [15]	6.48 $\pm$ 0.03	328.7

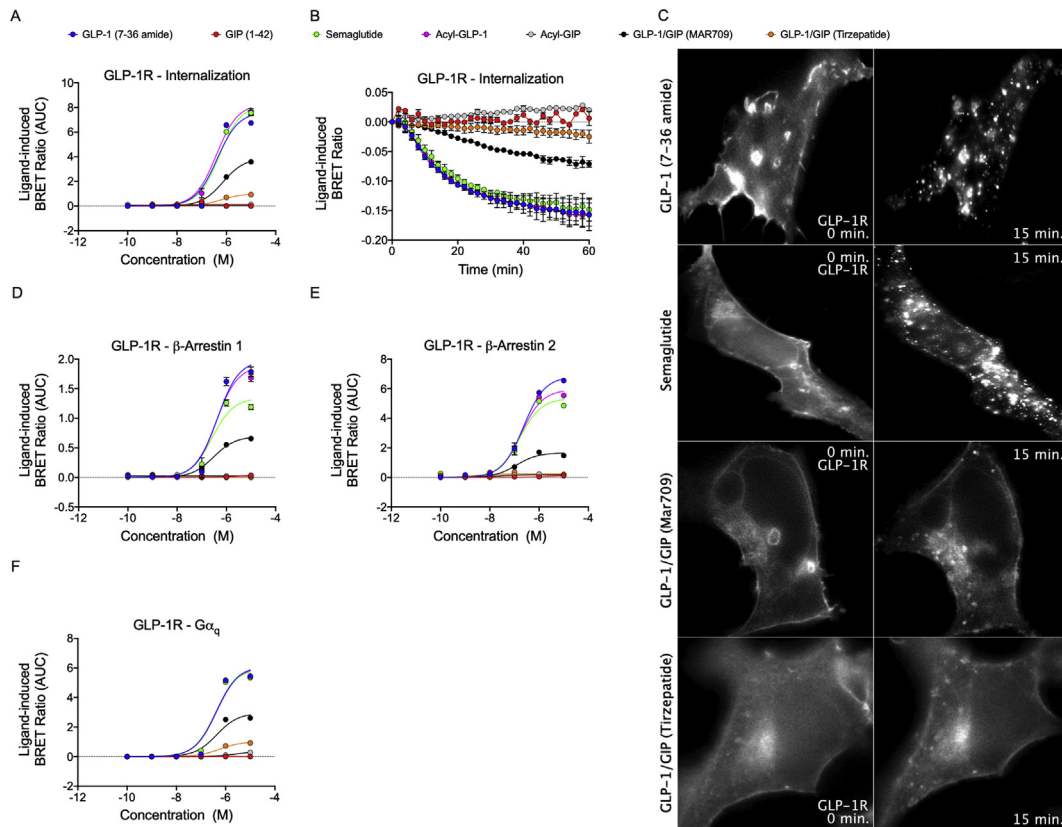


**Figure 4: Ligand-induced GLP-1R internalization.** Dose–response curves (A) and temporal resolution (1  $\mu$ M stimulation) (B) of ligand-induced hGLP-1-Rluc8 internalization as measured by loss of BRET with plasma membrane marker Venus-KRAS. Live HILO imaging of GLP-1R-GFP internalization in HEK293T cells at baseline and approximately 15 min after drug (1  $\mu$ M) treatment (representative image from  $n = 4$  experiments) (C). Dose–response curves for  $\beta$ -arrestin 1-Rluc8 (D),  $\beta$ -arrestin 2-Rluc8 (E), and  $G\alpha_q$ -Rluc8 recruitment (F) to GLP-1R-GFP. The  $\pm$  iAUC representation of vehicle and baseline-corrected 60 min (GLP-1R internalization and  $G\alpha_q$  recruitment) or 30 min ( $\beta$ -arrestin1/2 recruitment) temporal response to each agonist is expressed as mean  $\pm$  SEM. Three independent experiments were performed with at least two technical replicates per group.

recruitment  $E_{\max}$  elicited by GLP-1 (7–36 amide), while fatty acyl-GLP-1 elicited a slightly reduced 86% of  $\beta$ -arr2 (Figure 3D,E and Table 1). A pronounced reduction in  $\beta$ -arrestin recruitment efficacy with the dual-agonists was observed, in which treatment with MAR709 led to 35%

and 24% of the GLP-1 (7–36 amide)  $\beta$ -arr1 and  $\beta$ -arr2 recruitment  $E_{\max}$  (Figure 4D,E and Table 1), while no measurable response for either  $\beta$ -arr1 or  $\beta$ -arr2 was seen with tirzepatide (Figure 4D,E and Table 1).

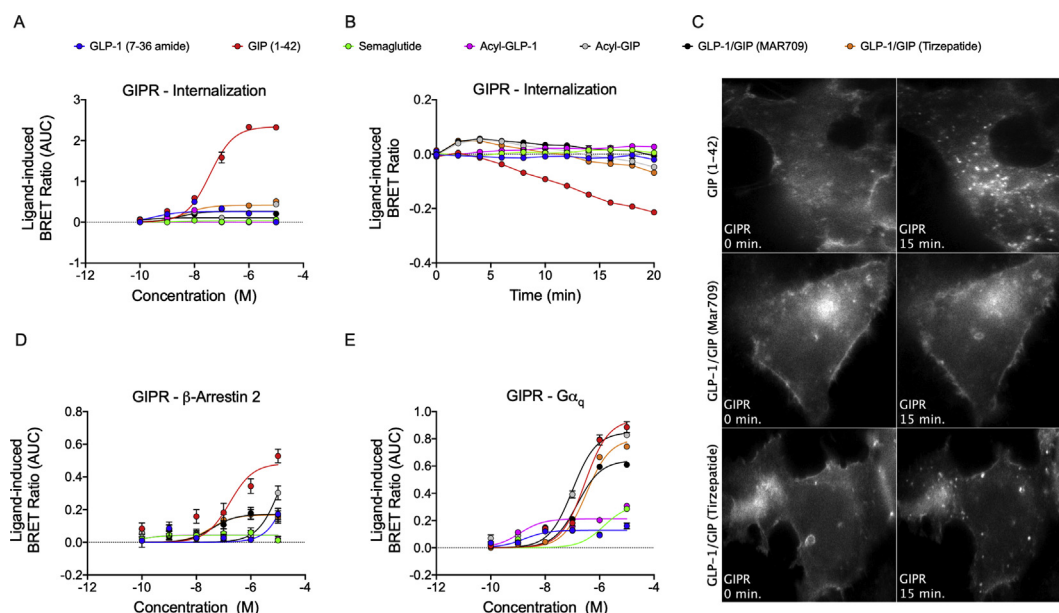


**Figure 5: Ligand-induced GIPR internalization.** Dose–response curves (A) and temporal resolution (1  $\mu$ M stimulation) (B) of ligand-induced hGIPR-Rluc8 internalization. Live HILO imaging of GIPR-GFP internalization in HEK293T cells at baseline and approximately 15 min after drug (1  $\mu$ M) treatment (C). Dose–response curves for  $\beta$ -arrestin 2-Rluc8 (D) and  $G\alpha_q$ -Nluc recruitment (E). The + iAUC representation of vehicle and baseline-corrected 20 min (GIPR internalization), 30 min ( $\beta$ -arrestin1/2 recruitment), or 60 min ( $G\alpha_q$  recruitment) temporal response to each agonist is expressed as mean  $\pm$  SEM. Three independent experiments were performed with at least two technical replicates per group.

GLP-1R recruitment of  $G\alpha_q$  has been proposed to regulate GLP-1R internalization via an ERK1/2 pathway [30]. In line with this data and our demonstration of decreased GLP-1R internalization upon treatment with MAR709 and tirzepatide (Figure 4A–C), we saw a less efficacious  $G\alpha_q$  recruitment response to the GLP-1R upon treatment with MAR709 and tirzepatide, in which 48% and 17% of the GLP-1 (7–36 amide)  $E_{max}$  was achieved, respectively (Figure 4F and Table 1).

In hGIPR<sup>+</sup> HEK293T cells, we observed sustained receptor internalization induced by GIP (1–42) but no meaningful internalization following treatment with either fatty acyl-GIP, the GLP-1 mono-agonists, or the dual-agonists (Figure 5A,B). In detail, MAR709 and tirzepatide stimulated 4% and 18% of the GIP (1–42) receptor internalization  $E_{max}$  (Figure 5A,B and Table 1). Reduced capacity of the dual-agonists for GIPR internalization was also confirmed visually through live-cell microscopy. Fifteen minutes after compound administration, GIP (1–42) showed a high dissolution of the GIPR-GFP-defined plasma membrane border with greater punctate structure formation in the cytosol, while neither MAR709 nor tirzepatide evoked a similar dynamic (Figure 5C).

Unlike  $\beta$ -arr2,  $\beta$ -arr1 has been shown to lack a functional role in GIPR internalization and trafficking [31]. Relative to GIP (1–42) at the maximal concentration of 10  $\mu$ M, a 36% and 35%  $\beta$ -arr2 recruitment response was observed in cells treated with MAR709 or tirzepatide (Figure 5D and Table 1). A true comparison between GIPR- $\beta$ -arr2 agonist  $E_{max}$  was not possible due to an incomplete curve fit for GIP (1–42). However, these data collectively suggested that reduced  $\beta$ -arrestin 2 recruitment by the dual-agonists may have had a functional correlation in the observed reduction in GIPR internalization or trafficking by these molecules.

Relative to the  $G\alpha_q$  recruitment  $E_{max}$  for GIP (1–42), treatment with fatty acyl-GIP displayed a similar efficacy while MAR709 and tirzepatide exhibited 68% and 85% of the maximal response (Figure 5E and Table 1). In summary, these data showed that MAR709 and tirzepatide both differed from the native peptides, semaglutide, and the PK-matched

receptor mono-agonists (fatty acyl-GIP and fatty acyl-GLP-1) in that they showed reduced internalization and decreased  $\beta$ -arrestin and  $G\alpha_q$  recruitment at both target receptors.

### 3.4. MAR709 and tirzepatide induced differential endosomal receptor trafficking relative to GLP-1R and GIPR mono-agonists

We next evaluated endosomal trafficking of the ligand-receptor complexes by assessing the co-localization of hGLP-1R-Rluc8 with Venus-tagged markers indicative of early endosomes (Rab5), late endosomes (Rab7), or recycling endosomes (Rab11) (Supplementary Figure 1). Consistent with our previous results showing decreased internalization of GLP-1R and GIPR by the dual-agonists (Figure 4A–C and Figure 5A–C), 1  $\mu$ M stimulation with MAR709 or tirzepatide resulted in 68% and 13% of the total GLP-1R Rab5 co-localization elicited by GLP-1 (7–36 amide) (Figure 6A–C). Similar patterns were also observed when assessing total  $G\alpha_s$  recruitment to GLP-1R<sup>+</sup> Rab5<sup>+</sup> endosomes (Supplementary Figure 2A–C). No difference in Rab5 co-localization was observed between GLP-1 (7–36 amide), semaglutide, and fatty acyl-GLP-1 (Figure 6A–C). In a hGLP-1R-Rluc8<sup>+</sup> min6  $\beta$  cell model, tirzepatide likewise stimulated reduced co-localization of GLP-1R into Rab5<sup>+</sup> endosomes compared to GLP-1 (7–36 amide) and GLP-1 mono-agonists (Supplementary Figure 5D–F). Within HEK293T cells, co-localization of GLP-1R with Rab7 positive (late) endosomes was reduced, with MAR709 and tirzepatide stimulating 62% and 24% of the response of GLP-1 (7–36 amide) (Figure 6D–F). This pattern was replicated in ligand-induced  $G\alpha_s$  recruitment to GLP-1R<sup>+</sup> Rab7<sup>+</sup> endosomes (Supplementary Figure 2D–F). Notably, differences in GLP-1R co-localization with Rab11-positive recycling endosomes were insignificant between treatments of MAR709 and GLP-1 (7–36 amide), but treatment with tirzepatide decreased by 54% (Figure 6G–I). Despite substantial  $G\alpha_s$  recruitment to Rab11<sup>+</sup> endosomes, endosomal  $G\alpha_s$  recruitment by MAR709 was significantly reduced compared to GLP-1 (7–36 amide) (Supplementary Figure 2F–I). Regarding the Min6 cell model, due to either a lack of BRET signals or



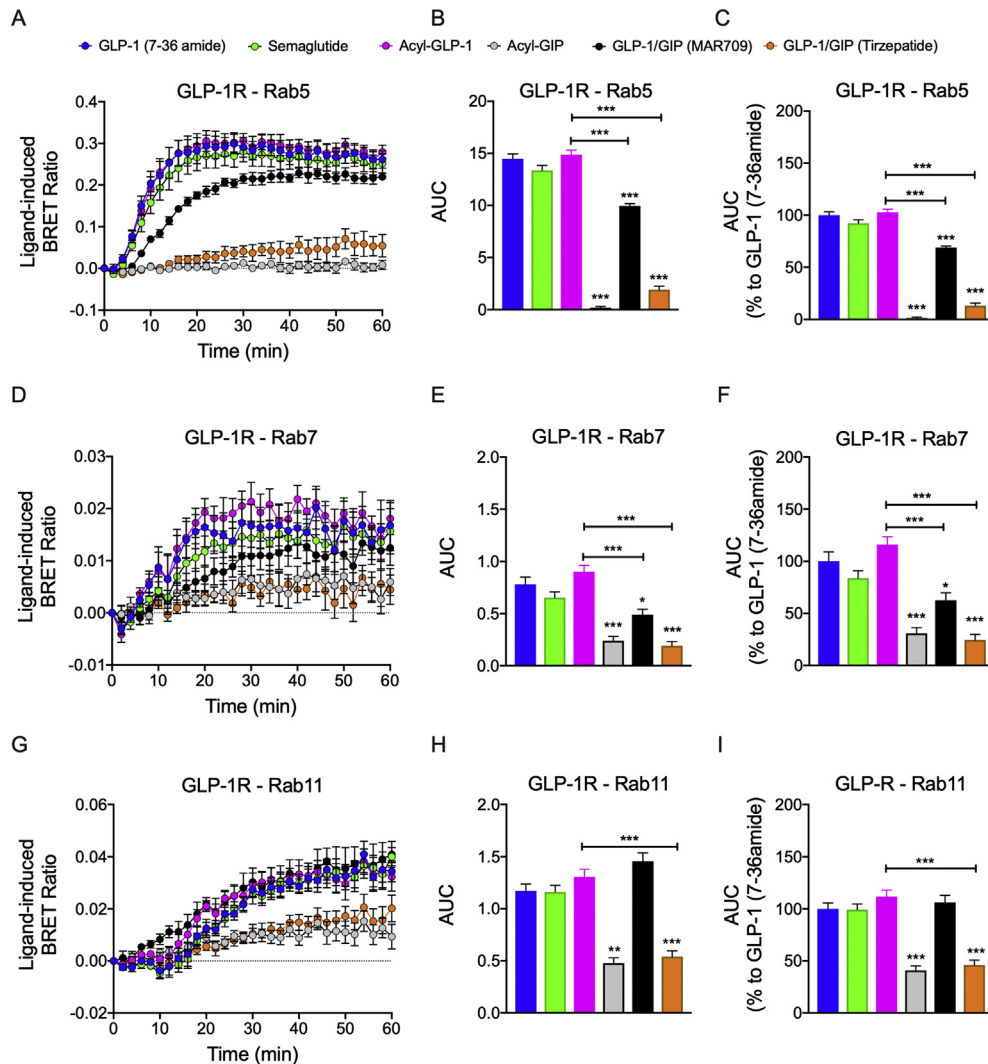


**Figure 6: Ligand-induced GLP-1R endosomal trafficking.** Ligand-induced co-localization of GLP-1R-Rluc8 with Venus-Rab5 early endosomes (A–C), Venus-Rab7 late endosomes (D–F), and Venus-Rab11 recycling endosomes (G–I). The + iAUC representation of vehicle and baseline-corrected temporal response to each agonist is expressed as mean  $\pm$  SEM. Bonferroni's test, \* $p < 0.05$ , \*\* $p < 0.005$ , and \*\*\* $p < 0.0005$  using one-way ANOVA vs GLP-1 (7–36 amide). Six independent experiments were performed with at least two technical replicates per group.

the requirement for improved detection sensitivity, replication of ligand-induced GLP-1R co-localization with Rab7- and Rab11-positive endosomes was not observable for any agonist (Supplementary Figure 5G–J). In HEK293T cells, the general agonist relationship between the AUC of GLP-1R endosomal co-localization and endosomal G protein recruitment was positively linear, in which greater endosomal trafficking was associated with greater  $G\alpha_s$  recruitment to the endosomal sub-compartment (Supplementary Figure 6A–C). In summary, these data indicated that MAR709 not only induced less GLP-1R co-localization into early and late endosomes but also comparably incorporated GLP-1R into Rab11<sup>+</sup> recycling endosomes to that of GLP-1 (7–36 amide) and semaglutide in HEK293T cells. In GIPR<sup>+</sup> HEK293T cells, GIPR co-localization into Rab5<sup>+</sup> endosomes was similar upon treatment with GIP (1–42), fatty acyl-GIP, and tirzepatide; however, MAR709 achieved approximately 66% of this response (Figure 7A,B). This pattern was also seen in  $G\alpha_s$  recruitment to Rab5<sup>+</sup> endosomes. No meaningful co-localization was detected with GIPR at either Rab7 or Rab11 (Figure 7C–F). The lack of receptor

co-localization with Rab7<sup>+</sup> and Rab11<sup>+</sup> endosomes was similarly associated with a lack of endosomal  $G\alpha_s$  recruitment (Supplementary Figure 3D–H). Discrepancies between GIPR Rab5<sup>+</sup> co-localization and the lack of GIP receptor internalization by the dual-agonists likely reflected methodological differences and/or lack of Rab5<sup>+</sup> early endosome scission from the plasma membrane.

#### 4. DISCUSSION

Our data showed that the GLP-1/GIP dual-agonists MAR709 and tirzepatide differed from the GLP-1R and GIPR mono-agonists in terms of G protein recruitment, target receptor internalization, and endosomal trafficking. Although both dual-agonists showed delayed internalization at both target receptors, MAR709 but not tirzepatide induced comparable GLP-1R accumulation into Rab11<sup>+</sup> recycling endosomes to that of GLP-1 (7–36 amide) and semaglutide. Both MAR709 and tirzepatide exhibited reduced  $G\alpha_s$  recruitment to the GLP-1R relative to GLP-1 (7–36 amide) while retaining full-agonist

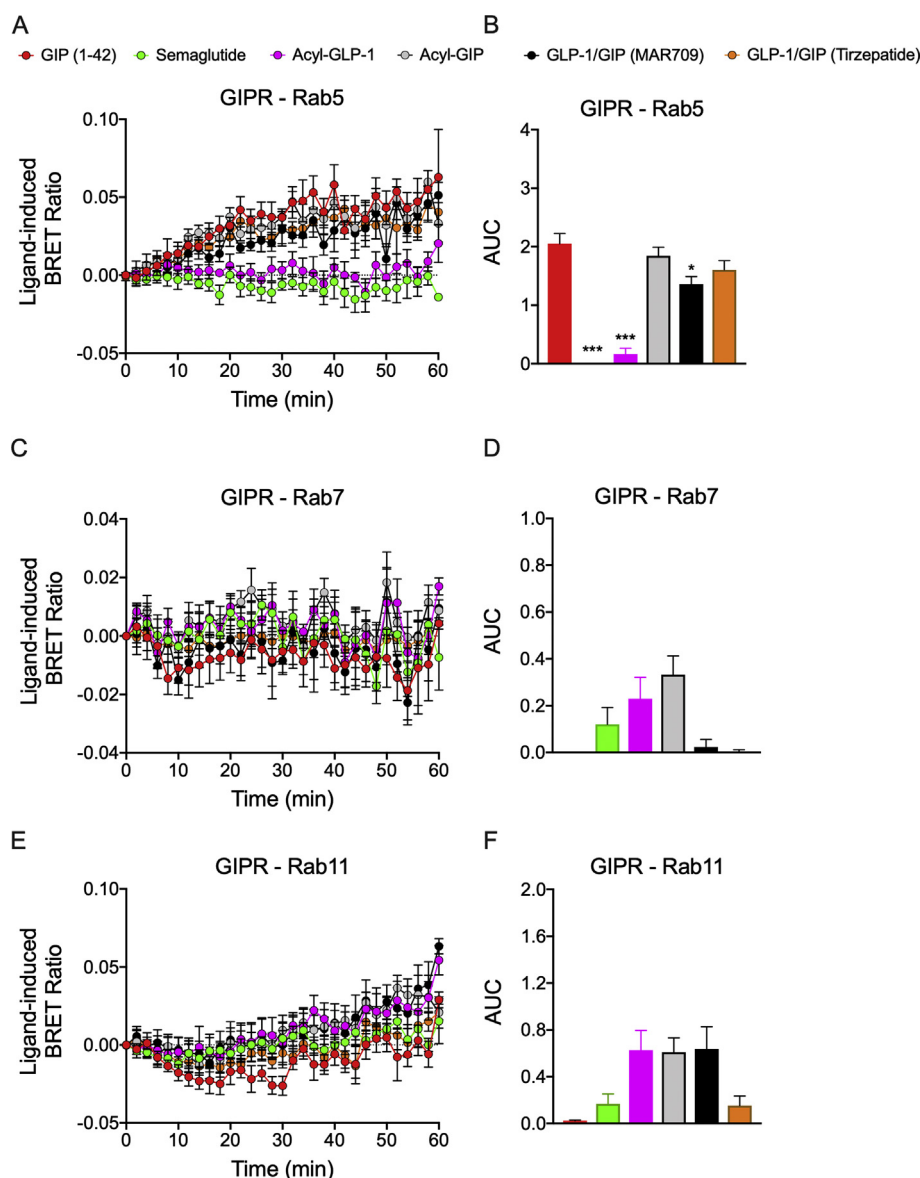


**Figure 7: Ligand-induced GIPR endosomal trafficking.** Ligand-induced co-localization of GIPR with Venus-Rab5<sup>+</sup> early endosomes (**A** and **B**), Venus-Rab7<sup>+</sup> late endosomes (**C** and **D**), and Venus-Rab11<sup>+</sup> recycling endosomes (**E** and **F**). The +iAUC representation of vehicle and baseline-corrected temporal response to each agonist is expressed as mean  $\pm$  SEM. Bonferroni's test, \* $p < 0.05$ , \*\* $p < 0.005$ , and \*\*\* $p < 0.0005$  using one-way ANOVA vs GIP (1–42). Six independent experiments were performed with at least two technical replicates per group.

capacity for cAMP, likely an advantageous effect of signal amplification systems. Similarly, both MAR709 and tirzepatide evidenced full agonism for cAMP at the GIPR, but only MAR709 displayed characteristics of partial agonism with a slight reduction in  $G\alpha_s$  recruitment efficacy. These data together were in line with previously established reports [19]. Since MAR709 and tirzepatide showed 100% sequence homology at positions 1–12, the observed differences between MAR709 and tirzepatide apparently resulted from sequence substitutions at positions 13–27 of the peptides or from the size and location of fatty acylation. The aforementioned differences in total and endosomal  $G\alpha_s$  recruitment may play a role in the endosomal sorting of the internalized receptor to Rab7<sup>+</sup>/lysosomal pathways [32].

GLP-1R internalization is primarily caveolin-1/dynamin dependent [33], mediated by  $G\alpha_q$  signaling [30], and does not require but is influenced by  $\beta$ -arrestin [16,34]. GLP-1R internalization has been linked to the

degree of cellular desensitization and insulin secretion in vitro [16,35]. Tirzepatide has previously been shown to elicit reduced GLP-1R internalization relative to native GLP-1 [36]. Whether this effect also holds true for other dual-agonists has yet to be demonstrated. Both dual-agonists evaluated herein retained a higher presence of GLP-1R at the plasma membrane relative to the tested GLP-1R mono-agonists and similarly displayed corresponding partial agonism for  $\beta$ -arrestin 1,  $\beta$ -arrestin 2, and  $G\alpha_q$  recruitment to the GLP-1R. A Phe1 substitution within an exendin-4 sequence has previously been described to reduce GLP-1R internalization and  $\beta$ -arrestin recruitment [16]. In line with this, reduced internalization is also observed with a (phenolic) Tyr1 present in the MAR709 and tirzepatide amino acid sequences. Both dual-agonists showed minimal GIPR internalization relative to GIP (1–42). Yet, both GIP (1–42) and tirzepatide elicited equal GIPR incorporation into Rab5<sup>+</sup> early endosomes. Reasons for the

discrepancy might have originated in the methodology of how internalization was assessed.

Ligand-induced GLP-1R endosomal trafficking has not yet been fully elucidated. We showed that MAR709 did not differ from GLP-1 (7–36 amide) and semaglutide in terms of eliciting GLP-1R co-localization with Rab11+ recycling endosomes. Whether this was a consequence primarily of internalized receptor diverting into recycling pathways or whether increased Rab11 co-localization induced by MAR709 was supplemented with recruitment of GLP-1R from the biosynthetic pathway has yet to be established. Given the low rate of GLP-1R internalization and incorporation into Rab5+ and Rab7+ endosomes, MAR709's high capacity for Rab11+ co-localization and its biased signaling profile demonstrated unique spatiotemporal pharmacology at the GLP-1R that may facilitate potential attributes of cellular sensitization. A caveat to the receptor trafficking experiments was the limited potential for aberrant Venus-Rab localization into non-specific endosomal compartments occurring from over-expression associated changes in Rab trafficking patterns. Additionally, transferability of these findings to physiologically relevant  $\beta$  cells was restricted to the min6  $\beta$  cell model, and hence represents a limitation of this work.

Despite favoring GIPR over the GLP-1R, tirzepatide showed comparable efficacy and potency relative to MAR709 at multiple signaling pathways connected to the GIPR, with the exception of cAMP pEC50 in which MAR709 exhibited higher potency. At the GLP-1R, MAR709 displayed higher  $G_{\alpha_s}/G_{\alpha_q}$  signaling, receptor internalization, and  $\beta$ -arrestin recruitment relative to tirzepatide despite still acting as a partial agonist in each of these categories. In addition, MAR709 elicited a disproportional incorporation of the GLP-1R into Rab11+ recycling endosomes. Collectively, our data showed that MAR709 and tirzepatide differed from the tested receptor agonists in G protein recruitment, receptor internalization, and endosomal trafficking, which together supports the hypothesis that biased agonism of these molecules might contribute to their beneficial metabolic action profile.

## AUTHOR CONTRIBUTIONS

A.N. and S.O'B. co-conceptualized the project, designed and performed the experiments, analyzed and interpreted the data, and wrote the manuscript. M.B., G.G., and M.K. conducted the experiments and analyzed and interpreted the data. P.K. performed peptide synthesis. A.Z., M.K., K.S., R.D.D., M.H.T., and B.F. co-conceptualized the project, interpreted the data, and revised the manuscript critically. D.C. and T.D.M. conceptualized and supervised the experiments, analyzed and interpreted the data, and wrote the manuscript.

## ACKNOWLEDGMENTS

This study was supported in part by funding from the Alexander von Humboldt Foundation, the Helmholtz Alliance *ICEMED*, the Helmholtz Initiative on Personalized Medicine *iMed* by the Helmholtz Association, the Helmholtz Cross-Program Topic Metabolic Dysfunction, and the Wellcome Trust (Wellcome Trust Senior Research Fellowship 212313/Z/18/Z to D.C.). This work was further supported by grants from the German Research Foundation TRR152, and TRR296, the European Research Council ERC AdG HypoFlam no. 695054, and the German Center for Diabetes Research (DZD e.V.).

## CONFLICT OF INTEREST

MHT is a member of the scientific advisory board of ERX Pharmaceuticals, Cambridge, MA, USA. He was a member of the Research Cluster Advisory Panel

(ReCAP) of the Novo Nordisk Foundation between 2017 and 2019. He attended a scientific advisory board meeting of the Novo Nordisk Foundation Center for Basic Metabolic Research, University of Copenhagen, in 2016. He received funding for his research projects by Novo Nordisk (2016–2020) and Sanofi-Aventis (2012–2019). He was a consultant for Bionorica SE (2013–2017), Menarini Ricerche S.p.A. (2016), and Bayer Pharma AG Berlin (2016). As former director of the Helmholtz Diabetes Center and the Institute for Diabetes and Obesity at Helmholtz Zentrum München (2011–2018), and since 2018, as CEO of Helmholtz Zentrum München, he has been responsible for collaborations with a multitude of companies and institutions worldwide. In this capacity, he discussed potential projects with and signed contracts for his institute(s) and the staff for research funding and/or collaborations with industry and academia worldwide, including but not limited to pharmaceutical corporations such as Boehringer Ingelheim, Eli Lilly, Novo Nordisk, MediGene, Arbrormed, BioSyngen, and others. In this role, he was/is further responsible for commercial technology transfer activities of his institute(s), including diabetes-related patent portfolios of Helmholtz Zentrum München such as, for example, WO/2016/188932 A2 or WO/2017/194499 A1. MHT confirmed that to the best of his knowledge, none of the funding sources were involved in preparing this paper. KS and TDM received research funding by Novo Nordisk, but these funds were unrelated to the work described herein. R.D.D. is a co-inventor on intellectual property owned by Indiana University and licensed to Novo Nordisk. He was previously employed by Novo Nordisk. B.F. and P.J.K. are current employees of Novo Nordisk.

## APPENDIX A. SUPPLEMENTARY DATA

Supplementary data to this article can be found online at <https://doi.org/10.1016/j.molmet.2021.101181>.

## REFERENCES

- [1] Muller, T.D., Finan, B., Bloom, S.R., D'Alessio, D., Drucker, D.J., Flatt, P.R., et al., 2019. Glucagon-like peptide 1 (GLP-1). *Molecular Metabolism* 30:72–130.
- [2] Deacon, C.F., Johnsen, A.H., Holst, J.J., 1995. Degradation of glucagon-like peptide-1 by human plasma in vitro yields an N-terminally truncated peptide that is a major endogenous metabolite in vivo. *Journal of Clinical Endocrinology & Metabolism* 80:952–957.
- [3] Kieffer, T.J., McIntosh, C.H., Pederson, R.A., 1995. Degradation of glucose-dependent insulinotropic polypeptide and truncated glucagon-like peptide 1 in vitro and in vivo by dipeptidyl peptidase IV. *Endocrinology* 136:3585–3596.
- [4] Mentlein, R., Gallwitz, B., Schmidt, W.E., 1993. Dipeptidyl-peptidase IV hydrolyses gastric inhibitory polypeptide, glucagon-like peptide-1 (7–36)amide, peptide histidine methionine and is responsible for their degradation in human serum. *European Journal of Biochemistry* 214:829–835.
- [5] De Meester, I., Korom, S., Van Damme, J., Scharpe, S., 1999. CD26, let it cut or cut it down. *Immunology Today* 20:367–375.
- [6] Meier, J.J., 2012. GLP-1 receptor agonists for individualized treatment of type 2 diabetes mellitus. *Nature Reviews Endocrinology* 8:728–742.
- [7] Muller, T.D., Clemmensen, C., Finan, B., DiMarchi, R.D., Tschöp, M.H., 2018. Anti-obesity therapy: from rainbow pills to polyagonists. *Pharmacological Reviews* 70:712–746.
- [8] Bettge, K., Kahle, M., Abd El Aziz, M.S., Meier, J.J., Nauck, M.A., 2017. Occurrence of nausea, vomiting and diarrhoea reported as adverse events in clinical trials studying glucagon-like peptide-1 receptor agonists: a systematic analysis of published clinical trials. *Diabetes, Obesity and Metabolism* 19.
- [9] Coskun, T., Sloop, K.W., Loghin, C., Alsina-Fernandez, J., Urva, S., Bokvist, K.B., et al., 2018. LY3298176, a novel dual GIP and GLP-1 receptor agonist for the treatment of type 2 diabetes mellitus: from discovery to clinical proof of concept. *Molecular metabolism* 18:3–14.

- [10] Finan, B., Ma, T., Ottaway, N., Müller, T.D., Habegger, K.M., Heppner, K.M., et al., 2013. Unimolecular dual incretins maximize metabolic benefits in rodents, monkeys, and humans. *Science Translational Medicine* 5.
- [11] Frias, J.P., Nauck, M.A., Van, J., Kutner, M.E., Cui, X., Benson, C., et al., 2018. Efficacy and safety of LY3298176, a novel dual GIP and GLP-1 receptor agonist, in patients with type 2 diabetes: a randomised, placebo-controlled and active comparator-controlled phase 2 trial. *Lancet*, 392 (London, England).
- [12] Miyawaki, K., Yamada, Y., Ban, N., Ihara, Y., Tsukiyama, K., Zhou, H., et al., 2002. Inhibition of gastric inhibitory polypeptide signaling prevents obesity. *Nature Medicine* 8.
- [13] Nauck, M.A., Heimesaat, M.M., Orskov, C., Holst, J.J., Ebert, R., Creutzfeldt, W., 1993. Preserved incretin activity of glucagon-like peptide 1 [7-36 amide] but not of synthetic human gastric inhibitory polypeptide in patients with type-2 diabetes mellitus. *Journal of Clinical Investigation* 91.
- [14] Killian, E.A., Wang, J., Yie, J., Shi, S.D., Bates, D., Min, X., et al., 2018. Anti-obesity effects of GIPR antagonists alone and in combination with GLP-1R agonists in preclinical models. *Science Translational Medicine* 10.
- [15] Holst, J.J., Rosenkilde, M.M., 2020. GIP as a therapeutic target in diabetes and obesity: insight from incretin Co-agonists. *Journal of Clinical Endocrinology & Metabolism* 105.
- [16] Jones, B., Buenaventura, T., Kanda, N., Chabosseau, P., Owen, B.M., Scott, R., et al., 2018. Targeting GLP-1 receptor trafficking to improve agonist efficacy. *Nature Communications* 9:1602.
- [17] Wootten, D., Reynolds, C.A., Smith, K.J., Mobarec, J.C., Koole, C., Savage, E.E., et al., 2016. The extracellular surface of the GLP-1 receptor is a molecular trigger for biased agonism. *Cell* 165.
- [18] Hager, M.V., Clydesdale, L., Gellman, S.H., Sexton, P.M., Wootten, D., 2017. Characterization of signal bias at the GLP-1 receptor induced by backbone modification of GLP-1. *Biochemical Pharmacology* 136:99–108.
- [19] Yuliantie, E., Darbalaei, S., Dai, A., Zhao, P., Yang, D., Sexton, P.M., et al., 2020. Pharmacological characterization of mono-, dual- and tri-peptidic agonists at GIP and GLP-1 receptors. *Biochemical Pharmacology* 177.
- [20] Finan, B., Ma, T., Ottaway, N., Muller, T.D., Habegger, K.M., Heppner, K.M., et al., 2013. Unimolecular dual incretins maximize metabolic benefits in rodents, monkeys, and humans. *Science Translational Medicine* 5, 209ra151.
- [21] Frias, J.P., Bastyr 3rd, E.J., Vignati, L., Tschop, M.H., Schmitt, C., Owen, K., et al., 2017. The sustained effects of a dual GIP/GLP-1 receptor agonist, NNC0090-2746, in patients with type 2 diabetes. *Cell Metabolism* 26:343–352 e342.
- [22] Coskun, T., Sloop, K.W., Loghin, C., Alsina-Fernandez, J., Urva, S., Bokvist, K.B., et al., 2018. LY3298176, a novel dual GIP and GLP-1 receptor agonist for the treatment of type 2 diabetes mellitus: from discovery to clinical proof of concept. *Mol Metab* 18:3–14.
- [23] Jiang, L.I., Collins, J., Davis, R., Lin, K.M., DeCamp, D., Roach, T., et al., 2007. Use of a cAMP BRET sensor to characterize a novel regulation of cAMP by the sphingosine 1-phosphate/G13 pathway\*. *Journal of Biological Chemistry* 282: 10576–10584.
- [24] Lan, T.H., Liu, Q., Li, C., Wu, G., Lambert, N.A., 2012. Sensitive and high resolution localization and tracking of membrane proteins in live cells with BRET. *Traffic* 13:1450–1456.
- [25] Porrello, E.R., Pfleger, K.D., Seeber, R.M., Qian, H., Oro, C., Abogadie, F., et al., 2011. Heteromerization of angiotensin receptors changes trafficking and arrestin recruitment profiles. *Cellular Signalling* 23.
- [26] Lan, T.H., Kuravi, S., Lambert, N.A., 2011. Internalization dissociates  $\beta$ 2-adrenergic receptors. *PLoS One* 6.
- [27] Fillion, D., Devost, D., Sleno, R., Inoue, A., Hébert, T.E., 2019. Asymmetric recruitment of  $\beta$ -arrestin1/2 by the angiotensin II type I and prostaglandin F2 $\alpha$  receptor dimer. *Frontiers in Endocrinology* 10.
- [28] Tiulpakov, A., White, C.W., Abhayawardana, R.S., See, H.B., Chan, A.S., Seeber, R.M., et al., 2016. Mutations of vasopressin receptor 2 including novel L312S have differential effects on trafficking. *Molecular Endocrinology* 30: 889–904.
- [29] Tian, X., Kang, D.S., Benovic, J.L., 2014.  $\beta$ -arrestins and G Protein-Coupled receptor trafficking. *Handbook of Experimental Pharmacology* 219:173–186.
- [30] Thompson, A., Kanamarlapudi, V., 2015. Agonist-induced internalisation of the glucagon-like peptide-1 receptor is mediated by the G $\alpha_q$  pathway. *Biochemical Pharmacology* 93.
- [31] Abdullah, N., Beg, M., Soares, D., Dittman, J.S., McGraw, T.E., 2016. Downregulation of a GPCR by  $\beta$ -Arrestin2-mediated switch from an endosomal to a TGN recycling pathway. *Cell Reports* 17:2966–2978.
- [32] Rosciglione, S., Thériault, C., Boily, M.O., Paquette, M., Lavoie, C., 2014. G $\alpha_s$  regulates the post-endocytic sorting of G protein-coupled receptors. *Nature Communications* 5.
- [33] Oh, P., McIntosh, D.P., Schnitzer, J.E., 1998. Dynamin at the neck of caveolae mediates their budding to form transport vesicles by GTP-driven fission from the plasma membrane of endothelium. *The Journal of Cell Biology* 141:101–114.
- [34] Sonoda, N., Imamura, T., Yoshizaki, T., Babendure, J.L., Lu, J.C., Olefsky, J.M., 2008. Beta-Arrestin-1 mediates glucagon-like peptide-1 signaling to insulin secretion in cultured pancreatic beta cells. In: *Proceedings of the national Academy of Sciences of the United States of America*, 105.
- [35] Baggio, L.L., Kim, J.G., Drucker, D.J., 2004. Chronic exposure to GLP-1R agonists promotes homologous GLP-1 receptor desensitization in vitro but does not attenuate GLP-1R-dependent glucose homeostasis in vivo. *Diabetes* 53(Suppl 3).
- [36] Willard, F.S., Douros, J.D., Gabe, M.B.N., Showalter, A.D., Wainwright, D.B., Suter, T.M., et al., 2020. Tirzepatide is an imbalanced and biased dual GIP and GLP-1 receptor agonist. *JCI insight*.